PCCP

Accepted Manuscript

This is an *Accepted Manuscript*, which has been through the Royal Society of Chemistry peer review process and has been accepted for publication.

Accepted Manuscripts are published online shortly after acceptance, before technical editing, formatting and proof reading. Using this free service, authors can make their results available to the community, in citable form, before we publish the edited article. We will replace this *Accepted Manuscript* with the edited and formatted *Advance Article* as soon as it is available.

You can find more information about *Accepted Manuscripts* in the Information for Authors.

Please note that technical editing may introduce minor changes to the text and/or graphics, which may alter content. The journal's standard Terms & Conditions and the Ethical guidelines still apply. In no event shall the Royal Society of Chemistry be held responsible for any errors or omissions in this *Accepted Manuscript* or any consequences arising from the use of any information it contains.

ROYAL SOCIETY OF CHEMISTRY

www.rsc.org/pccp

Journal Name ARTICLE

Enhancement of carbon supports available specific surface area for boosting the electroactivity of nanostructured Pt catalysts

Yaovi Holade,[a] Claudia Morais,[a] Karine Servat,[a] Teko W. Napporn,[a] and K. Boniface Kokoh*[a]

Abstract. We report the increasingly improvement of the available specific surface area of the widespread used Vulcan XC 72R and Ketjenblack EC-600JD carbons by simple thermal pre-treatment. The treated Vulcan and Ketjenblack substrates show a specific surface area of 322 and 1631 $m^2\ g^{-1}$ respectively instead of 262 and 1102 $m^2\ g^{-1}$ for the as-received materials, meaning 23 and 48 % of improvement. Subsequently, when used as platinum nanoparticles (3 nm) supports, the electrochemical active surface area is enhanced by a factor of 2.2 and 1.2 for treated Vulcan and Ketjenblack carbons, respectively. Furthermore, the electrochemical investigations have highlighted a surprisingly better catalytic activity for the pre-treated Vulcan XC 72R and Ketjenblack EC-600JD supported Pt nanoparticles. In fact, the synthesized nanostructures from the so-called "Bromide Anion Exchange" method exhibit good catalytic activity toward glucose electrooxidation both in alkaline medium and phosphate buffered solution at pH 7.4. More importantly, the present catalysts are four times more active than those in the literature prepared under similar conditions for glucose dehydrogenation at low potential (0.27 V *vs*. Reversible Hydrogen Electrode). Consequently, these remarkable trends uncovered herein provide ample new strategic routes for the pre-treatment of Vulcan 72R and Ketjenblack carbons for widespread utilizations.

Physical Chemistry Chemical Physics Accepted Manuscript

This journal is © The Royal Society of Chemistry 2014

PCCP RSCPublishing

ARTICLE

1. Introduction

From the energy conversion and storage systems to chemicals synthesis, carbon based-materials play major roles.[1-4] Amongst all chemical elements, carbon is undoubtedly the widely used one. Recently, Friedman has reviewed the potential uses of carbon by the expression "The four words of carbon".[5] The carbon based-materials find their major applications in catalysis as nanoparticles supports[2,3,5-7] despite their potential direct uses.[2,3,6-8] When used in catalysis in general, two major roles are assigned to the carbon based-materials such as Vulcan, Ketjenblack, nanotubes, nanofibers, buckypaper, graphene etc. The first is the reduction of the active metal loading by dispersing it on the carbon substrate, employed as support, the percentages ranging from *ca*. one to dozens. In such targets, the support must have a large available active surface area. That is why the preparation of carbon materials with high available surface area is of great interest. The second purpose is the potential synergistic effect between the chemical species present on its surface and the deposited metal nanoparticles. This is well known as "support effect".[9-12] To be used in electrochemistry (batteries, fuel cells and electrosynthesis), these carbon materials must fulfil a third condition: to be a good electronic conductor. Both Vulcan XC 72R and Ketjenblack carbons satisfy these conditions. To be in line with the first condition, various methods have focused on the improvement of the available specific surface area of carbon materials.[13,14]

To date, it was reported that Vulcan carbon is annealed at 400 °C under nitrogen atmosphere before its utilization as support of metal nanoparticles,[15,16] in order to clean it[17] or remove the undesired contaminants, like sulphur, coming from its industrial manufacturing.[18] Grolleau et al.[17] have reported that the heat treatment of Vulcan XC 72 carbon led to change of its specific surface area from 237 to 314 $m^2 g^{-1}$. Unfortunately, there are no sound studies describing the effect on the catalytic performances. In the middle of 90s, Krishnankutty and Vannice have reported the modification of the physicochemical properties of carbon black (Black Pearls 2000, 1475 $m^2 g^{-1}$), such as surface area, porosity, and adsorption properties after thermal or chemical pre-treatment.[18] To our knowledge, it still remains little information about the specific surface state of Vulcan or Ketjenblack carbons when submitted to this thermal process. The correlation of this pre-treatment process with the physicochemical properties of the support and so far the reactivity of the catalyst is a very important task since the Vulcan and Ketjenblack carbon materials become the cornerstones in the fields of fuel cell science and batteries.[19-22] Vulcan carbon is well known to be an excellent catalysts support in many applications from fuel cells to batteries. But the electrochemical interest of Ketjenblack carbon is becoming widespread because the nanoparticles deposited onto its surface have shown remarkable catalytic activities.[23-26]

The purpose of the present study is to propose a simple and commode process for the enhancement of the available specific surface area of the commercial Vulcan XC 72R and Ketjenblack EC-600JD carbon materials. Then, the effect of this thermal pre-treatment on their physicochemical properties will be investigated and the correlation of these properties with catalytic behaviours will be attempted. To these ends, a simple thermal pre-treatment has been set up. The as-received and home-treated carbon materials were used as supports during the preparation of platinum nanoparticles. The physicochemical properties of the free supports and supports containing platinum nanoparticles were scrutinized by various techniques such as nitrogen (N_2) adsorption-desorption isotherms, Raman spectroscopy, differential/thermogravimetric analysis (DTA/TGA), X-ray diffraction (XRD) and transmission electron microscopy (TEM). Finally, the catalytic activity of the as-synthesized nanostructures was thoroughly evaluated electrochemically using glucose as oxidative probing molecule in fuel cell system.

2. Experimental

2.1 Thermal treatment of the carbon materials under nitrogen atmosphere

The carbon materials used herein were Vulcan XC 72R carbon black purchased from Cabot and Ketjenblack EC-600JD supplied by Akzo Nobel Polymer Chemicals (B.V., Amersfoort, Netherlands). To perform their thermal pre-treatment, an amount of the commercial materials was put in a Pyrex crucible and introduced in a closed furnace under nitrogen atmosphere. The level of the thermal pre-treatment was 400 °C. So, to reach this level, the temperature of furnace containing the sample was raised at rate of 5 °C min^{-1}. After 4 h of operating, the furnace was cooled. In any study herein, the as-received (untreated) Vulcan XC 72R and Ketjenblack EC-600JD will be appointed as C-nt and KB-nt, respectively. In the same time, our homemade thermal pre-treated Vulcan XC 72R and Ketjenblack EC-600JD will be represented as C and KB, respectively.

2.2 The use of the carbon materials as platinum nanoparticles supports

As aforementioned, we have used herein separately four carbon materials C-nt, C, KB-nt, and KB as supports of platinum (Pt) nanoparticles. So, the obtained catalysts will be named as Pt/C-nt, Pt/C, Pt/KB-nt and Pt/KB, respectively. Unless the use of Pt

Physical Chemistry Chemical Physics Accepted Manuscript

becomes restrictive due to its rarity and cost, it is the state-of-art material for the evaluation of the catalytic performances.[21,27-29] Therefore a low Pt loading of 20 wt.% was used for the catalysts formulation. The so-called Bromide Anion Exchange (BAE) method[30-33] was slightly modified herein to prepare these carbon supported nanostructures. The main feature of this method lies on its simplicity. Without any organic compounds as surfactant, clean, small, and well-dispersed active nanoparticles for catalytic applications were obtained. In a standard procedure, the BAE method consists of the reduction of Pt(IV) ions in aqueous solution in the presence of bromide ion as capping agent. Typically, 53.1 mg of chloroplatinic acid hexahydrate ($H_2PtCl_6 \cdot 6H_2O$) purchased from Sigma-Aldrich® (ACS reagent ≥ 37.50 % Pt basis) were dissolved in a reactor containing 100 mL of ultrapure water (Milli-Q® Millipore, 18.2 MΩ cm at 293 K) thermostatted at 25 °C under stirring. Then, 17.8 mg of potassium bromide (KBr, ≥ 99 %) supplied by Sigma-Aldrich® were added under vigorous stirring. Afterwards, a suitable amount of the appropriate carbon, untreated or previously pre-treated, as stated above, was added under constant ultrasonic homogenization for 45 min. After adding dropwise the reducing agent, i.e. 15 mL of sodium borohydride (0.1 mol L^{-1} $NaBH_4$) purchased from Sigma-Aldrich® (99 %), the mixture was kept under vigorous stirring for 2 h. Finally, the supported materials were filtered, washed several times with ultra pure water and dried in oven at 40 °C for 12 h.

2.3 Physicochemical characterization of the material powder

The four kinds of carbon materials textural properties were accessed by the N_2 adsorption-desorption isotherms recorded at liquid N_2 temperature (77.3 K). The evaluation of the specific surface area was made following the Brunauer-Emmett-Teller (BET) theory.[6] This specific surface area (S_{BET} in m^2 g^{-1}) was calculated by considering relative pressure ranging from 0.05 to 0.16 P/P^0 during the adsorption process. Furthermore, the Barrett, Joyner and Halenda (BJH) method from nitrogen adsorption isotherm using the modified Kelvin equation with the relative pressure of 0.2-0.99 P/P^0 was employed to establish the pore size distribution (PSD). To assess the micropores data, the method known as t-plot in lower relative pressure during the adsorption process (0-0.2 P/P^0) was employed.[18,34,35] Otherwise, before performing the experiment, *ca*. 40 mg of the sample was degassed and heat-treated at 90 °C for 1 h followed by 350 °C for 4 h minimum under high vacuum conditions. Finally, the measurements were fulfilled on Micrometrics ASAP 2010 instruments.

The investigation of carbon species that are present in/on these carbon based-materials was performed by Raman spectroscopy. A HORIBA Jobin Yvon Labram HR800UV Raman spectrometer equipped with a CCD detector cooled by Peltier effect was used. The excitation wavelength was 514.5 nm and was produced by an Ar^+ laser (Melles Griot). A filter of optical density was employed in order to limit the sample irradiation by laser at power of 0.05 mW. Furthermore, the Raman instrument was coupled to an Olympus microscope with a 100 × microscope objective. The spectral resolution was 1.5 cm^{-1}. Prior to the analysis, the spectrometer was calibrated with a silicon sample. For analysis, a few milligrams amount of sample is deposited onto a glass slide. Then, three spectra are recorded on three different areas for each sample. LabSpec 5 software was used for data acquisition and analysis.

In supported material synthesis science, the knowledge of the final metal loading and information on thermodynamics of the involved reactions is most commonly obtained by coupling thermogravimetric analysis (TGA) to differential thermal analysis (DTA). DTA/TGA was achieved with the TA Instruments SDT Q600 apparatus equipped with TA Universal Analysis software. Basically, two alumina crucibles, one containing *ca* 7 mg of the sample and another empty (reference) were thermally heated under air flow of 100 mL min^{-1} from 25 to 900 °C with a temperature rate of 5 °C min^{-1}.

Material structure understanding provides relevant information on its catalytic properties.[36] In this approach, the crystal structure and the crystallite size of the thermal treated carbon substrates and the homemade nanomaterials were performed by XRD measurements on an ENPYREAN (PANanalytical) diffractometer in Bragg-Brentano (θ-θ) configuration with a copper tube powdered at 45 kV and 40 mA ($Cu_k\alpha_1$ = 1.54060 Å and $Cu_k\alpha_2$ = 1.54443 Å). To avoid the interference from the kβ component, a nickel filter was installed in a secondary optic. The diffraction angle (in 2θ) from 15 to 140 ° was investigated in step mode, with steps of 0.05 °and fixed acquisition time of 2 min/step. Raw data were analysed with the HighScorePlus® software using the Pseudo-Voigt function.[37]

Furthermore, the particles dispersion on the support and their size were accessed by TEM analysis. The measurements were conducted in a TEM/STEM JEOL 2100 UHR (200 kV) equipped with a LaB_6 filament. Then, ImageJ® free software[38,39] was used as tool to get the size distribution and mean particle size by measuring the diameter of at least 700 isolated particles.

2.4 Electrochemical measurements

All electrochemical experiments reported herein were fulfilled on an analogical potentiostat EG&G PARC Model 362 (Princeton Applied Research) in a conventional three-electrode Pyrex cell.[40-42] The reversible hydrogen electrode (RHE), separated from the solution by a Luggin capillary tip was used as reference electrode. The H^+/H_2 equilibrium was prepared prior to each electrochemical experiment by electrolysis of a solution from the daily supporting electrolyte (see below). The counter electrode was a glassy carbon slab of 6.48 cm^2 geometric surface, whereas the working electrode consisted of a catalytic ink (3 µL) deposited onto a glassy carbon disk of 3 mm diameter, previously polished with alumina powder (1 µm and 0.05 µm). The catalytic ink preparation according to the procedure initiated by Wilson and co-workers [43] for fuel cells applications was well described elsewhere.[32,33] The cyclic voltammetry (CV)[40,42] experiments in alkaline medium were achieved in 0.1 mol L^{-1} NaOH as supporting electrolyte, provided by Sigma-Aldrich® (ReagentPlus, 97 %) or in 0.2 mol L^{-1} phosphate buffered solution (PBS) at pH 7.4. PBS was prepared from sodium dihydrogen phosphate monohydrate ($NaH_2PO_4 \cdot 2H_2O$, ACROS ORGANICS; ≥ 99 %) and disodium hydrogen phosphate (Na_2HPO_4, Fluka Biochemika; ≥ 99.5 %) salts. Herein, all named ultra pure water was Milli-Q® Millipore (18.2 MΩ cm at 20 °C). Furthermore, the electrolyte solution was deoxygenated by bubbling high quality of nitrogen (Air Liquide) for 30 min before any electrochemical experiment in order to avoid any dissolved oxygen interferences during electrochemical measurements. The anodic catalytic activity of the as-synthesized nanostructures was investigated by using 10 mmol L^{-1} glucose (D-(+)-glucose, Sigma-Aldrich®, 99.5 %) in 0.1 mol L^{-1} NaOH or in 0.2 mol L^{-1} PBS. In the CVs, the currents were normalized with the metal weight value accessed

Physical Chemistry Chemical Physics Accepted Manuscript

through TGA analysis in order to provide more correlation when these materials will be used in fuel cell systems.

3. Results and discussion

3.1 Nitrogen adsorption-desorption and Raman spectroscopy of carbon supports

The first physical method used herein to investigate the carbon materials was the N_2 adsorption-desorption. This technique allows the assessment of porous materials textural properties by using N_2 as probing molecule. The solid porous materials are classified according to their pore sizes[44] in three different categories: macroporous (> 50 nm), mesoporous (2-50 nm) and microporous (< 2 nm).[18,34,35] Figs. 1a and 1b show the adsorption-desorption isotherms of N_2 on the as-received and pre-treated carbon materials. The presence of mesopores is evidenced by the slightly hysteresis loop characteristic of capillary condensation at higher pressure.[18,34,35] This phenomenon is more pronounced on KB-nt and KB, successively, than C-nt and C. The difference in the desorption profiles of Vulcan and Ketjenblack carbon substrates is certainly due to the mesoporous volume. The shape of the steep initial branch at lower pressures indicates the presence of micropores in the sample. The different parameters are summarized in Table 1. The pore radius evaluated from Joyner and Halenda method (R_{BJH}) as aforementioned increases as follows: C-nt (1.82 nm) < C (1.86 nm) < KB-nt (2.01 nm) < KB (2.02 nm), and corresponds to mesoporous materials with mean pore sizes ranging from 3.64 to 4.04 nm. Besides, the materials also exhibit microporous character whose the determined volume represents 15.6, 24.2, 1.2 and 1.6 % of the total pore volume for C-nt, C, KB-nt and KB, respectively. We notice that, in the case of C-nt and C for the total volume, the variations observed upon thermal treatment might be within the experimental error of the determination rather than a true annealing effect. However, the obtained results highlight an increase in the microporous volume of the thermally treated samples when compared to the as-received ones. The origin of this enhancement may be the removal of some "impurities" resulted in the industrial manufacturing process, which can block the pores. Sulfur is one of these suspected species because its content in carbon materials can exceed 1.3 wt.%.[18] Because of the important role of the pores, this feature will strongly affect the diffusion and adsorption properties. Furthermore, there is a highly improvement of the specific surface areas that attain 322 and 1631 $m^2\ g^{-1}$ for C and KB, respectively compared to 262 and 1102 $m^2\ g^{-1}$ for the as-received C-nt and KB-nt, respectively. Compared to the commercial materials, the S_{BET} values of the thermally pre-treated materials represent 123 % (C) and 148 % (KB) *i.e.* 60 and 529 $m^2\ g^{-1}$ of specific surface gained for C and KB, respectively. Because of the removal of some species like sulphur, potential catalyst poising agent, the process developed herein could find suitable applications in all domains using Vulcan or Ketjenblack carbon substrates and could even be extended to others kinds of carbon-based materials.

Otherwise, Raman spectroscopy was also used to get insights on the nature of the carbon species present in/on the carbon-based materials. To obtain such information from the raw data, the decomposition of the Raman spectra was performed using pseudo-bands Voigt function. The Raman shifts of the bands D (Disorder) and G (Graphitic) as well as the graphitization indices (I_D/I_G) for the different materials were then accessed.[45-52] Figs. 2a and 2b display the recorded spectra and Table 1 summarizes the data of interest. The decomposition reveals four contributions. The first band localized around 1602 cm^{-1} is typically called G-mode, corresponding to the E_{2g} symmetry.[45,47,50,53] Information provided by this band concerns the in-plane vibration of the sp^2-bonded carbon atoms (C=C stretching vibrations).[46,48,49,53] The so-called D mode appears in the 1343-1352 cm^{-1} range for the different studied materials. It is also named as D-band (A_{1g} symmetry) and results from the symmetry breakdown for carbon atoms situated at the edge of graphite sheets.[15,47,54,55] Whereas the Raman shift for the G band is nearly the same for the four materials, there are slight differences for the D band, indicating small differences in carbon atoms located at the edge of graphite sheets. The amorphous sp^2 phase of carbon appears at *ca*. 1518 cm^{-1} between the bands G and D.[49,50,53] Finally, the origin of the band centred at 1180 cm^{-1} has been successively assigned to nanocrystalline diamond,[55] hexagonal diamond [56] and more recently to the sp^3 rich phase.[51] These four observed bands correspond to those already reported for Vulcan XC 72 and Vulcan XC 72R carbons,[15,49] but not yet for Ketjenblack EC-600JD. The degree of graphitization of these carbonaceous materials (I_D/I_G ratio) is used to quantify both the amount of defects in the carbon-based materials as well as the in-plane crystallite size (*La*) [15] *via* Eq. (1).[57] For Vulcan carbon, the I_D/I_G ratio was found to slightly decrease from 2.14 to 2.11, while *La* increases from 7.86 to 7.97 nm. The trend is the same for Ketjenblack carbon for which the I_D/I_G ratio varies from 2.00 to 1.97, whereas *La* increases from 8.41 to 8.54 nm. The first ascertainment concerns the magnitude of these two fundamental parameters. They are the same than those previously obtained for Vulcan carbon.[15,49] Besides, a slight decrease of I_D/I_G can be observed for the pre-treated materials, as already stated.[15]

$$La\ (\text{nm}) = \left(2.4.10^{-10}\right)\lambda^4 \left(\frac{I_D}{I_G}\right)^{-1} \qquad (1)$$

where λ is the laser wavelength in nm.

Physical Chemistry Chemical Physics Accepted Manuscript

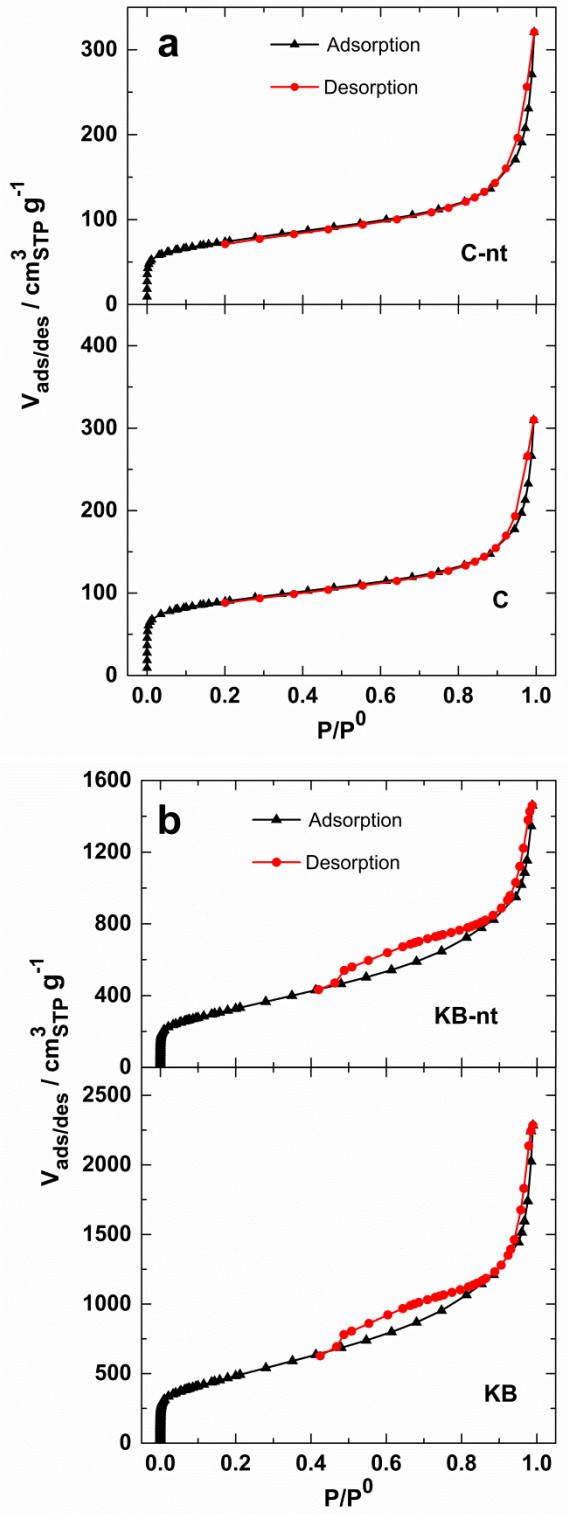

Figure 1 N_2 adsorption-desorption isotherms at -196 °C for as-received (top) and thermally pre-treated (down) carbon materials (a) Vulcan XC 72R and (b) Ketjenblack EC-600JD.

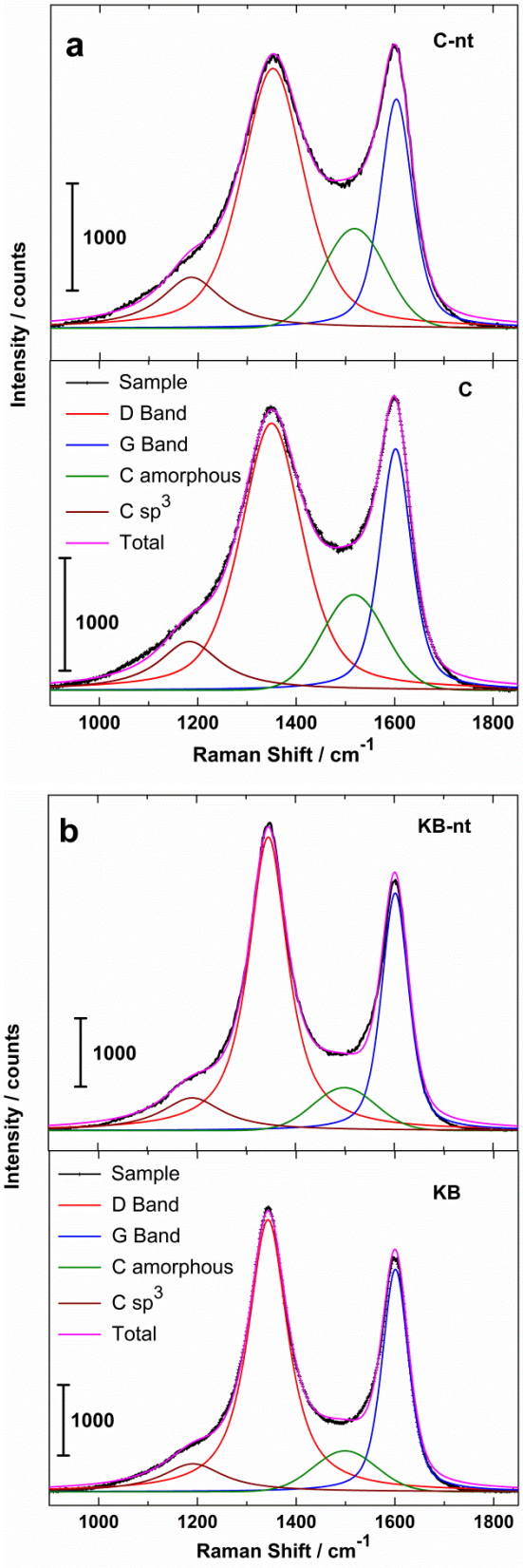

Fig 2 Raman spectra of the as-received (top) and thermally pre-treated (down) carbon materials (a) Vulcan XC 72R and (b) Ketjenblack EC-600JD.

Physical Chemistry Chemical Physics Accepted Manuscript

Table 1: Supports physicochemical properties: BET and Raman spectroscopy

		C-nt	C	KB-nt	KB
N_2 adsorption-desorption	S_{BET} ($m^2 g^{-1}$)	262	322	1102	1631
	R_{BHJ} (nm)	1.82	1.86	2.01	2.02
	V_{total} ($cm^3 g^{-1}$)	0.32	0.33	1.68	2.47
	V_{micro} ($cm^3 g^{-1}$)	0.05	0.08	0.02	0.04
	V_{meso} ($cm^3 g^{-1}$)	0.27	0.25	1.66	2.43
Raman spectroscopy	υ_D (cm^{-1})	1352	1350	1345	1343
	υ_G (cm^{-1})	1603	1602	1602	1601
	I_D/I_G	2.14	2.11	2	1.97
	La (nm)	7.86	7.97	8.41	8.54
Material aspect (powder)		Pellets		Granulated	

3.2 TGA-TDA, XRD and TEM analyses of Pt/C Materials

The four carbon-based materials previously described were used herein as supports of Pt nanoparticles. To access the accurate metal loading of each material, TGA-DTA experiments were conducted. Before analysing the supported materials, TGA (Fig. 3a) and DTA (Fig. 3b) measurements of C and KB alone were performed to further explore their influence in the presence of nanoparticles. The exothermic/endothermic character of the reaction occurring is represented by the DTA plots in Fig. 3b. Basically, positive and negative peaks in DTA plot indicates involved exothermic and endothermic reactions, respectively. The peak positions are gathered in Table 2. The combustion of Vulcan and Ketjenblack carbon substrates starts at *ca*. 450 °C followed by an exothermic peak at 648 and 628 °C for C and KB, respectively. Sellin et al.[58,59] have recently analysed the influence of Pt nanoparticles on the Vulcan XC 72 carbon combustion by thermogravimetry and mass spectrometry. It was surprisingly found that this reaction was catalysed by Pt nanoparticles, because this peak position shifted importantly toward lower temperatures.[58,59] As highlighted by Figs. 3a and 3b, this phenomenon can be extended to Ketjenblack. Indeed, the peak associated with the carbon combustion shifts remarkably toward lower temperatures for the Pt/C-nt (421 °C), Pt/C (428 °C), Pt/KB-nt (451 °C) and Pt/KB (451 °C). More importantly, the reaction occurs earlier when Vulcan carbon is used as support, which can be due to the structure of the substrate and/or the Pt nanoparticles size. For temperature values close to 475 °C, a strange behaviour in the TGA curves is observed, which has consequences on the DTA results. The obtained shape is different to other reported metals such as Pd/C, Ag/C and Ni/C[32] or Au/C. Scrutiny was done in this temperature range during TGA analysis and surprisingly the same trend was observed. It may therefore be stated that this behaviour is an intrinsic property of Pt.[58,59] Finally, the expected metal loadings of the studied catalysts were found to be close to the targeted 20 wt. % value. The chemical synthesis yield of the obtained nanomaterials is reported in Table 2. As can be seen, all the yields are higher than 90 %, reaching 99 % for the Pt/KB material. This important result places BAE at the top of methods when considering the minimization of noble metal loss during the synthesis.

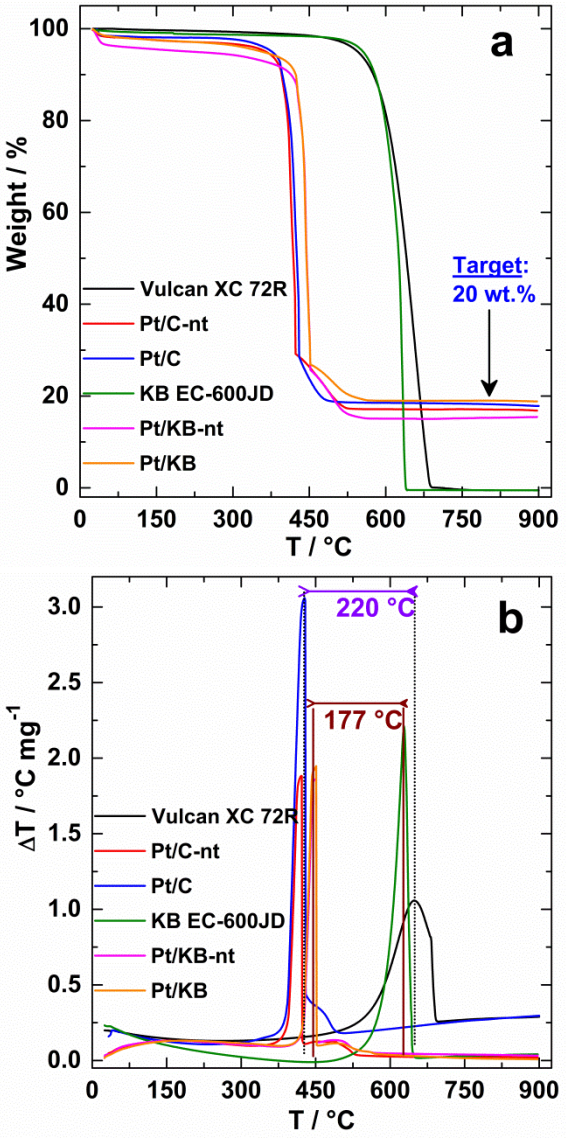

Figure 3. TGA (a) and DTA (b) curves at 100 mL min^{-1} air flow and 5 °C min^{-1} linear temperature variation of the carbon support and with the nanoparticles.

C, KB and carbon supported Pt nanoparticles were also characterized by XRD. The XRD patterns of C and KB are shown in Figure 4a. The peak at *ca*. 25 ° corresponds to

Physical Chemistry Chemical Physics Accepted Manuscript

graphite (002) crystallographic plane of carbon (XRD reference code 98-002-8419) and the one at 43 ° corresponds to (111) crystallographic plane of diamond (XRD reference code 98-004-4101). These characteristic peaks confirm the Raman investigations, indicating the presence of graphite and diamond in Vulcan and Ketjenblack carbon substrates. Otherwise, Figure 4b depicts the indexed XRD pattern of Pt/KB. The peaks at 39.84 °, 46.30 °, 67.73 °, 81.56 °, 86.29 °, 103,95 °, 118.50 ° and 123.55 ° correspond, respectively to the planes (111), (200), (220), (311), (222), (400), (331) and (420) of face-centred cubic (fcc) of Pt in the Pt/KB material. No Pt oxide phase is observed from XRD analysis. Besides, Fig. 4c displays the patterns of all supported nanoparticles, exhibiting the same fcc crystallographic structure. Different relations and equations were used to extract basic data from the patterns like crystallite size (L_V) and lattice parameter.[60,61] The parameter L_V was accessed through Debye-Scherrer equation (Eq. 2). It is worthy of note that is basically derived for a sample of cubic crystals, but as mentioned by Chatterjee,[61] it is applied to peak breadths of non cubic materials. The lattice parameter was determined by two methods: interplanar spacing of crystallographic plane (hkl) method (Eq. 4) and Bragg's law[62] (Eq. 5), which combines Eq. 3 and Eq. 4. The findings are summarized in Table 2 and Table S1 in the Electronic Supplementary Information (ESI).

$$L_V = \frac{k}{\beta \cos\theta} \quad (2)$$

$$\lambda = 2d_{(hkl)} \sin\theta \quad (3)$$

$$a_{(hkl)} = d_{(hkl)} \sqrt{h^2 + k^2 + l^2} \quad (4)$$

$$a_{(Bragg)} = \frac{\sqrt{h^2 + k^2 + l^2}}{2\sin\theta} \times \lambda \quad (5)$$

In these equations, λ is the wavelength of X-ray (1.54060 Å); a is the lattice parameter; θ is the Bragg's angle; β is the full width in radians subtended by at half maximum intensity; k is a constant, based on the assumption of small cubic crystals of uniform size, k = 0.93944;[61,63] L_V is the average crystallite size; $d_{(hkl)}$ is the interplanar spacing of crystallographic plane (hkl).

For all Pt nanoparticles, the obtained lattice parameter is smaller than the bulk (3.924 Å).[64] This contraction effect has been attributed to quantum size effect.[64-68] It is well known that the decrease of the particles size in nanomaterials affects strongly both the melting point of the metal and the crystalline lattice parameter.[9,69-71] Indeed, due to the surface tensions, the decrease of the particles size induces the contraction of the crystalline lattice parameter. Theoretical calculations reported by Swaminarayan et al.[72] showed that this shrinkage is inversely proportional to the size of the particle. Eq. 6 shows the relative variation of the lattice parameter (Δa/a) [9, 64].[64] Several experimental results have substantiated this phenomenon.[64,67] According to this equation, the contraction would result in the high pressure (χ factor) that the external environment exercises toward the centre of the particle and the high surface stresses (factor g). Moreover, this contraction effect, probably due to the decrease in the number of nearest neighbours of the surface atoms, would affect the valence electrons distribution in a smaller number of metallic bonds.[67]

$$\frac{\Delta a}{a} = -\frac{2\chi g}{3r} \quad (6)$$

where g is the surface stress, χ is the compressibility, r is the average radius of the particle, a is the lattice parameter of the bulk and Δa is the change of a due to the surface stress.

The average crystallite size evaluated for Pt/C-nt, Pt/C, Pt/KB-nt and Pt/C is between 3 and 4 nm. A rigorous determination of L_V requires to consider a diffraction angle from 30 to 50 °/2θ,[32,73] *i.e.* (111) and (200) planes. Furthermore, Debye-Scherrer equation is inappropriate for very small crystallites (< 3-4 nm). In fact, when the size is too small, phenomena like size effect and strain contributions strongly affect the broadening of the diffraction profile and thereby the integral breadth in accordance with "Williamson-Hall plot".[60,61]

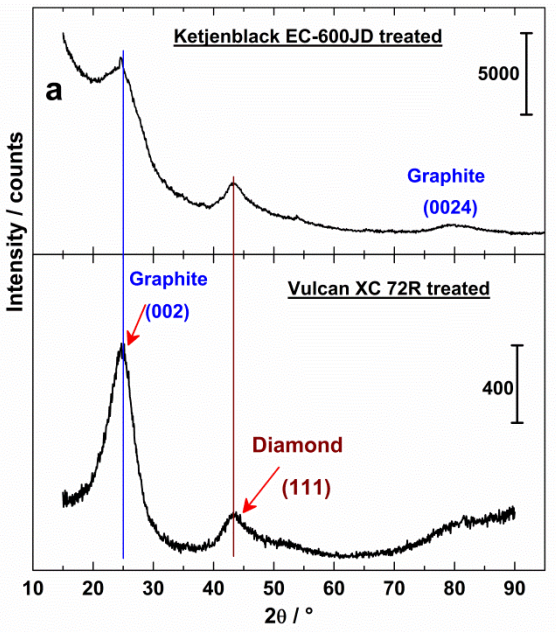

Physical Chemistry Chemical Physics Accepted Manuscript

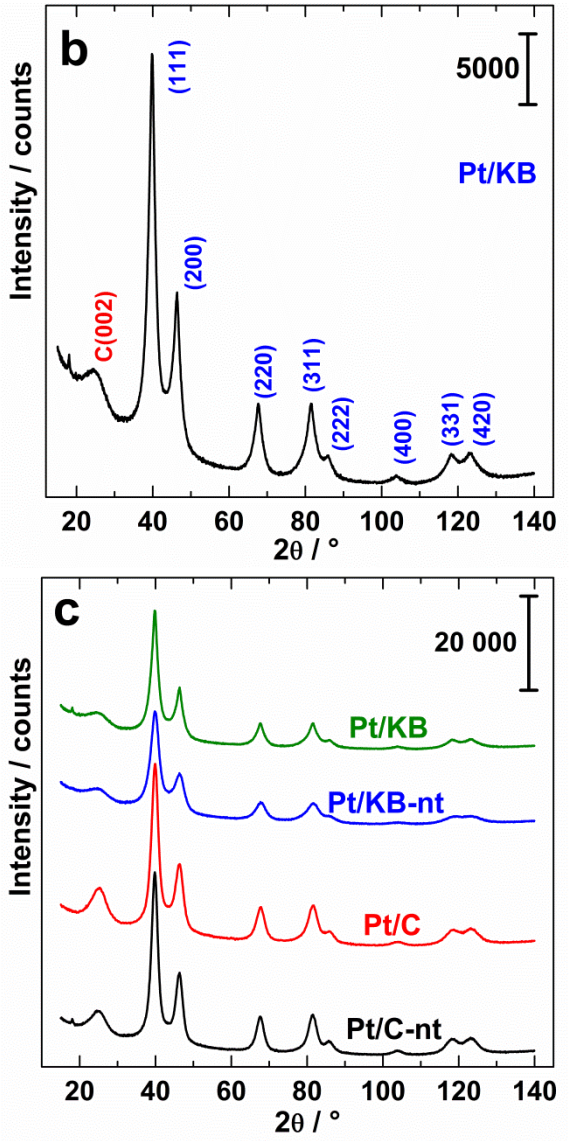

Figure 4. Indexed XRD patterns of (a) carbon materials used as supports and (b) Pt/KB. (c) XRD patterns of the different supported nanostructures.

To gain further insights on the nanoparticles distribution, TEM experiments were performed, as shown in Figs. 5 a, 5c, 5e and 5g. From these TEM images, very small and well-dispersed particles were observed, which is in fair line with the obtained XRD results. The high resolution micrographs are reported in Fig. S1 and highlights an octahedron-like shape for nanoparticles. As aforementioned, the mean particle size ($D_{m,p}$) was evaluated by considering the most representative number (> 700 isolated particles) and fitting the histograms using a LogNormal function.[74] Figs. 5b, 5d, 5f and 5h depict the histograms that exhibit the same $D_{m,p}$ value close to 3 nm for the four kinds of supported Pt materials. For comparison, the mean particle size of the total number of particles (N) was calculated from the following statistic formulae: arithmetic average size of N particles (D_m: Eq. 7); average particle size normalized with the surface of N particles (D_s: Eq. 8); average size normalized with the volume of N particles (D_v: Eq. 9).

$$D_m = \frac{\sum_{i=1}^{N} n_i d_i}{\sum_{i=1}^{N} n_i} \quad (7)$$

$$D_s = \frac{\sum_{i=1}^{N} n_i d_i^3}{\sum_{i=1}^{N} n_i d_i^2} \quad (8)$$

$$D_V = \frac{\sum_{i=1}^{N} n_i d_i^4}{\sum_{i=1}^{N} n_i d_i^3} \quad (9)$$

i: considered physical particle; d_i: diameter of particle i; n_i: number of particles of diameter d_i; N: total number of particles; average size of N particles; average particle size normalized with the surface of N particles; average size normalized with the volume of N particles.

The resulted values are summarized in Table 2. The value of D_m is close to that of $D_{m,p}$, which supports the hypothesis of the "quasi-spherical" trend of particles. In general, L_V is higher than $D_{m,p}$, and the gap between the two parameters becomes more important when the size of particles is lower than 5 nm. Besides, the values of D_s and D_v are bigger than $D_{m,p}$. This trend is expected unsurprisingly because the average size of the nanoparticles obtained from TEM analysis and evaluated statistically follows the order $D_m < D_s < D_v$.

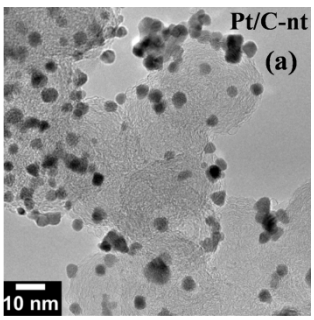

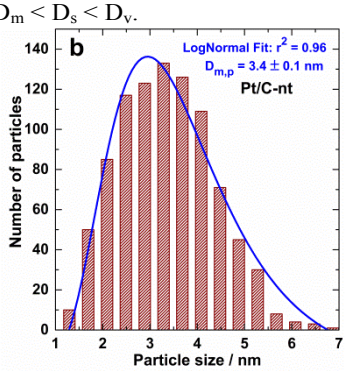

Physical Chemistry Chemical Physics Accepted Manuscript

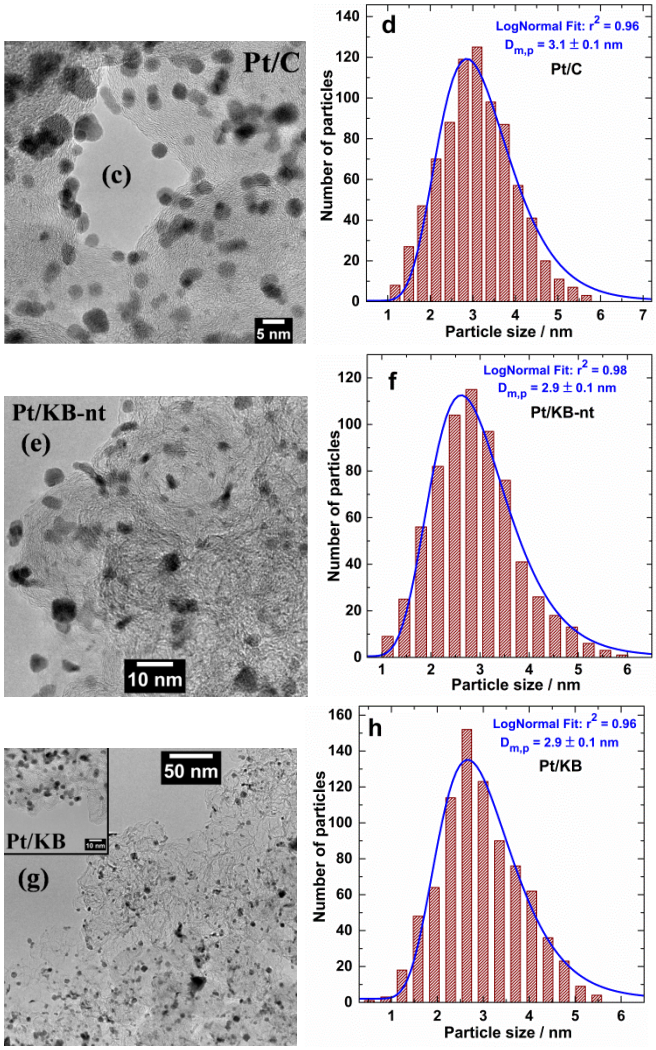

Figure 5. (a, c, e, g) TEM micrographs and (b, d, f, h) Particles size distribution.

Table 2: Physicochemical characterizations: DTA-TGA, XRD and TEM results

Technique	Parameters	C	Pt/C-nt	Pt/C	KB	Pt/KB-nt	Pt/KB
DTA-TGA	T_{peak} (°C)	648	421	428	628	451	451
	Metal loading (wt.%)	-	17	18	-	16	19
XRD	L_V (nm)	-	4.29	3.93	-	3.13	2.85
	$a_{(111)}$ (Å)	-	3.917	3.916	-	3.917	3.914
	$a_{(Bragg)}$ (Å)	-	3.915	3.907	-	3.910	3.915
TEM	D_m (nm)	-	3.3	3.1	-	2.9	2.9
	D_s (nm)	-	3.9	3.5	-	3.4	3.4
	D_v (nm)	-	4.1	3.7	-	3.6	3.7
	$D_{m,p}$ (nm)	-	3.4	3.1	-	2.9	2.9
Catalyst synthesis yield (%)		-	97	91	-	97	99

3.3 Electrochemical characterization of the carbon materials

First of all, the electrochemical behaviours of C-nt and KB-nt were investigated in 0.1 M NaOH by coating the glassy carbon with their ink. The corresponding CVs are depicted in Fig. 6. The current response was normalized with the carbon loading and the geometrical surface area of the glassy carbon substrate. The different CVs recorded at 10, 20, 50 and 100 mV s^{-1} scan rates are also reported in Figs. S2a and S2b. The shape of the voltammograms of the carbon electrodes recorded in alkaline medium is due to the quinone species. In Fig. S2c (pretreated Vulcan XC 72R carbon), the quinone/hydroquinone redox groups (located at the ends of graphene planes in Vulcan XC 72R carbon) with two exchanged electrons are noticeable at *ca.* 0.5 V *vs.* RHE during the forward going scan and at 0.4 V *vs.* RHE during the backward scan.[75] In term of comparison, the anodic (current > 0) and the cathodic (current < 0) charges are not equal, which indicates that the reactions involved during the positive and negative going-scans, respectively, are not reversible. At around 1.3 V *vs.* RHE the increase in current densities is not only due to the oxygen evolution reaction, but likely also to the carbon oxidation to CO_2 (herein carbonate).[76]

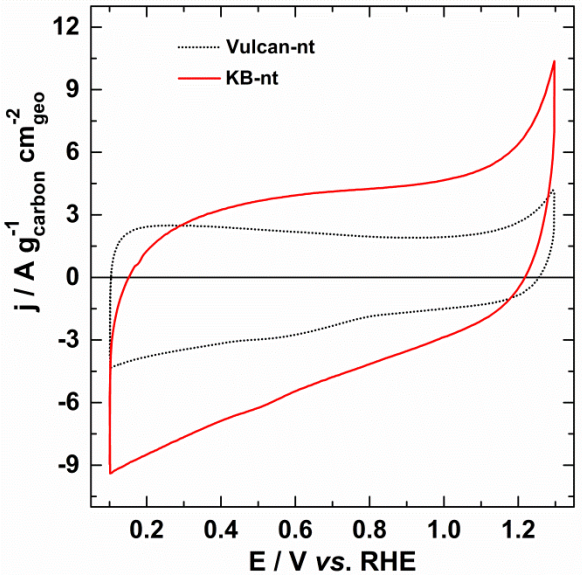

Figure 6. Cyclic voltammograms recorded in a N_2-satured 0.1 mol L^{-1} NaOH solution at 25 °C of the as-received carbon substrates at 20 mV s^{-1}.

3.4 Supported nanomaterials surface characterization by electrochemical measurements

Physical Chemistry Chemical Physics Accepted Manuscript

While the BET technique determines the total specific surface area of a material, the electrochemical measurement by cyclic voltammetry allows assessing the surface area of the nanoparticle active sites. This powerful and characteristic electrochemical tool was used for determining the specific electrochemical active surface areas (SECSA) of the carbon supported Pt catalysts. To this end, CVs were recorded in the supporting electrolyte (0.1 M NaOH). We describe in the Supplementary Information (graphically illustrated by Figs. S3a and S3b) the method used herein for the assessment of SECSA. Fig. 7 depicts the steady-state CVs recorded at scan rate of 50 mV s^{-1}. The hydrogen desorption from Pt sites occurs during the positive potential going-scan between 0.05 and 0.4 V *vs*. RHE, followed by the double layer charging current until 0.7 V *vs*. RHE and finally the Pt surface oxidation at higher potentials. In the reverse scan (current < 0) the Pt oxide reduction corresponding to the cathodic peak takes place at 0.7 V *vs*. RHE. Then, the Pt free surface becomes covered by adsorbed hydrogen in the lower potential region (from 0.4 to 0.05 V *vs*. RHE). The SECSA values obtained at 50 mV s^{-1} scan rate are plotted in Figure 8 and compared with the previously discussed BET surface areas. These values are 25, 55, 35 and 43 m^2 g^{-1} for Pt/C-nt, Pt/C, Pt/KB-nt and Pt/KB respectively. Subsequently, the Pt nanoparticles supported on the home-treated carbons exhibit enhancements of 120 and 23 % in the SECSA values when compared to the as-received Vulcan and Ketjenblack samples, respectively. This surprising improvement of SECSA is undoubtedly attributable to support-Pt interaction because the catalysts exhibit the same particle size, as evidenced by TEM and XRD characterizations. So, not only the thermal pre-treatment process improves the BET surface, but also does contribute to good interaction between the Pt nanoparticles and the support, leading to an enhanced SECSA, and corollary, to a highly exalted catalytic activity.

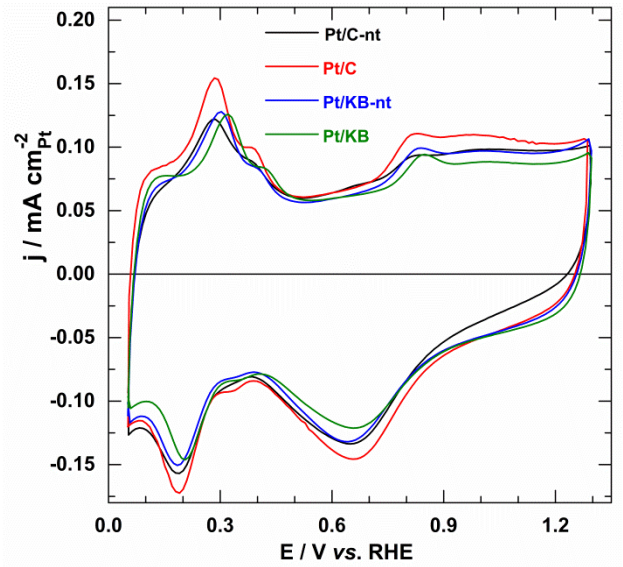

Figure 7. CVs recorded in 0.1 mol L^{-1} NaOH at 25 °C and 50 mV s^{-1} for Pt nanoparticles supported on Vulcan and Ketjenblack carbon substrates.

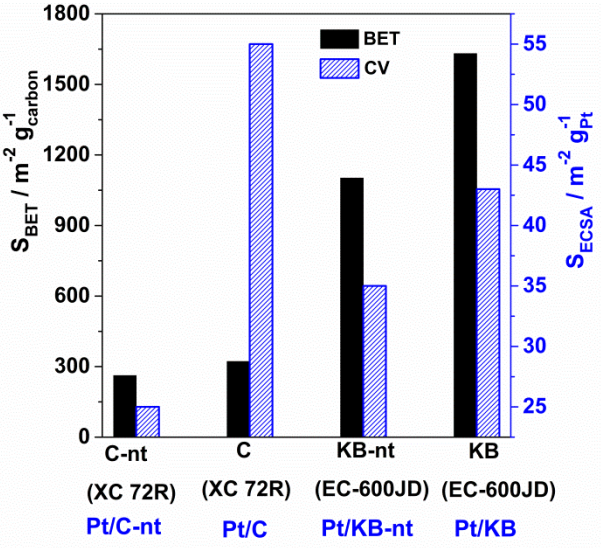

Figure 8. S_{BET} of the carbon support (black, left Y-axis) and SECSA of Pt (blue hatched, right Y-axis).

3.5 Electrochemical activity toward glucose oxidation

With the aim of investigating the catalytic performances of the different materials, the glucose electrooxidation was conducted in alkaline and neutral media. Carbohydrates are of great interest as they are sustainable and available compounds. They can be used in conventional alkaline fuel cell (FC) [77] or as fuel in biofuel cells (BFCs) for sensing or medical implants.[78-80] To improve the stability to the enzymatic or microbial BFCs, nanoscale abiotic materials were proposed for the oxidative glucose conversion.[81] The polarization curves in 0.1 M NaOH are shown in Fig. 9a for Pt/C-nt and Pt/C, and Fig. 9b for Pt/KB-nt and Pt/KB. From Fig. 9a, it can be concluded undoubtedly that the Pt nanoparticles supported on as-treated Vulcan present an improved catalytic activity, which is in agreement with the previous ECSA observations. The peak centred at 0.27 V *vs*. RHE corresponds to the glucose dehydrogenation, while that at *ca*. 0.7 V *vs*. RHE is associated with either the glucose oxidation at the Pt hydroxide surface, or that of the glucose reaction products such as gluconate.[30,82,83] The dehydrogenation peak shows a mass current of 22, 31, 23 and 28 A g^{-1} for Pt/C-nt, Pt/C, Pt/KB-nt and Pt/KB, respectively. This means that the capability of dehydrogenating the glucose molecule increases in the order Pt/C-nt ≈ Pt/KB-nt < Pt/KB < Pt/C. In some extent, Pt/C activity is 4 times higher than previously reported results [30] and highly improved compared to other findings in the literature.[77,83] For the peak current centred at *ca*. 0.7 V *vs*. RHE, the order is Pt/C-nt (50 A g^{-1}) < Pt/KB-nt (66 A g^{-1}) < Pt/KB (70 A g^{-1}) ≈ Pt/C (72 A g^{-1}). The remarkable improvement of the activity for the treated Vulcan carbon substrate can be attributed to the BET surface. Simply, this means that there is a value for the available BET surface of the support which leads to the better dispersion and interaction with the Pt nanocatalysts. Obviously, the normalization of the polarization curves in Figs. 9a and 9b by the Pt active surface area (current density in mA cm^{-2}_{Pt}) leads to

Physical Chemistry Chemical Physics Accepted Manuscript

a new trend where Pt nanoparticles supported on the pristine carbon substrates show better performance toward glucose electrooxidation (see Figs. S4a and S4b). This difference can be explained by the size of the glucose molecule. SECSA was determined using "H", which is very smaller than glucose molecule. Thus, some active sites (probably in micropores) are not accessible by the glucose molecule. Consequently, Pt/C (SECSA: 55 m^2 g^{-1}) displays lower current density than Pt/C-nt (SECSA: 25 m^2 g^{-1}). As can be seen in Figs. S4c and S4d, the resulted current during glucose electrooxidation is much important with the pretreated carbon substrates than the as-received ones. In practical application as anode material in fuel cell, the most important thing is the produced current. In this way, Pt/C and Pt/KB are better than Pt/C-nt and Pt/KB-nt, respectively. Please note that in most articles related to organic molecules electrooxidation for fuel cell applications, the electrode catalysts are compared in term of mass current (A g^{-1}) or current density using the geometrical surface area (mA $cm^2_{geometric}$).

Finally, the glucose electrooxidation in 0.2 M PBS at physiological pH (7.4) was investigated on the best catalyst evidenced in alkaline medium: Pt/C. Fig. 9c displays the CVs recorded without (black dotted line) and in the presence of 10 mM glucose (red solid line). The catalyst exhibits good activity even if in this buffered medium, adsorbed phosphate anions may occupy more catalytic sites than adsorbed species in alkaline medium (NaOH). Indeed, the electrochemical reactivity of alcohol based-compound increases with the pH value of the supporting electrolyte. Regarding the obtained results in alkaline and buffered electrolytic solutions, it may be concluded that Pt/C and Pt/KB are promising anode materials in glucose alkaline FC or hybrid BFC.

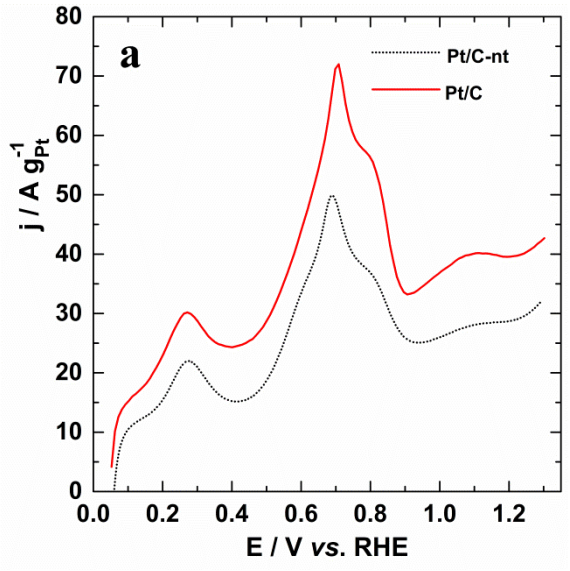

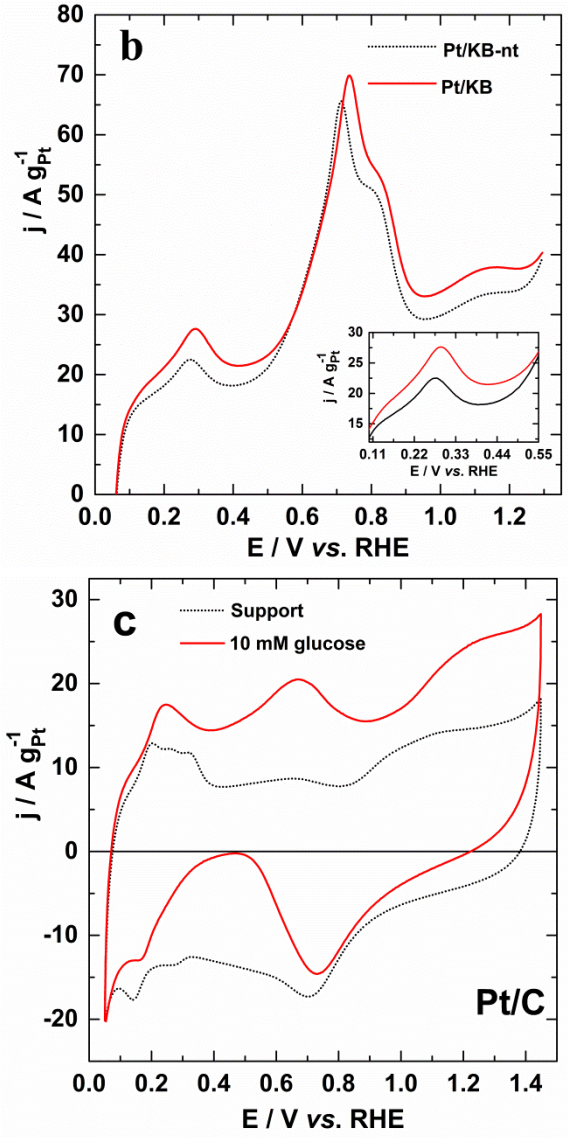

Figure 9. Polarisation curves recorded at 20 mV s^{-1} in 0.1 mol L^{-1} NaOH + 10 mmol L^{-1} glucose at 25 °C with (a) Vulcan XC 72R and (b) KB EC-600JD as supports. Inset (b): zoom of 0.10-0.55 V *vs.* RHE region. (c) CVs recorded in a N_2-satured 0.2 mol L^{-1} PBS solution (black dotted line) and in the presence of 10 mmol L^{-1} glucose (red solid line) at 37 °C on Pt/C at 20 mV s^{-1}.

4. Conclusions

In this work, effect aspects of the thermal pre-treatment of the commercial Vulcan XC 72R and Ketjenblack EC-600JD carbon substrates under nitrogen atmosphere at 400 °C were investigated. The physicochemical characterization of the as-received and treated carbon materials by nitrogen adsorption-desorption isotherms revealed a significant enhancement of BET surface of the treated materials. Actually, the BET surfaces of the treated materials were enhanced by 23 and 48 %, respectively for Vulcan and Ketjenblack, which have been attributed to the removal of some species that blocked the pores. The carbon materials were subsequently used as supports for platinum nanoparticles synthesized from the "Bromide

Physical Chemistry Chemical Physics Accepted Manuscript

Anion Exchange" approach. X-ray diffraction, transmission electron microscopy and cyclic voltammetry were then undertaken to gain further insights on the structural and electrochemical properties of the as-prepared nanoscale platinum materials. Finally, their catalytic performances toward the glucose electrooxidation were evidenced in alkaline and neutral media. It was found that the described physical pre-treatment strongly affects not only the physicochemical properties of the carbon materials, but also the catalytic electroactivity of the nanoparticles deposited onto their surface. Indeed the electrochemical active surface area has more than doubled, *i.e.* it increased from 25 to 55 $m^2 g^{-1}$ when as-received Vulcan was replaced by the pre-treated sample. As a consequence, treated carbon supported platinum nanomaterials exhibited highly exalted catalytic activities toward the glucose electrooxidation. Particularly, for glucose dehydrogenation at low electrode potential (0.27 V *vs*. RHE), the present catalysts are four times more active than similar reported electrocatalysts but thoroughly pretreated. The thermal pre-treatment proposed herein represents therefore a promising process to enhance the available specific surface of the carbon based-materials. This will undoubtedly be useful for a wide range of catalytic applications requiring large BET surfaces.

Acknowledgements

All authors acknowledge and thank the financial support of the French National Research Agency (ANR) through the program "ChemBio-Energy".

Notes and references

[a] *Université de Poitiers, UMR CNRS 7285, « Équipe SAMCat », 4, rue Michel Brunet, B27, TSA 51106, 86073 Poitiers cedex 09, France.*
Fax: +33 549 45 35 80; Tel: +33 549 45 41 20; E-mail: boniface.kokoh@univ-poitiers.fr.

Electronic Supplementary Information (ESI) available: Table S1 (whole XRD data of the catalysts) , HRTEM images, description of the method used for the electrochemical surface area (ECSA) evaluation, the as-recorded glucose electrooxidation polarization curves with their normalization with ECSA. See DOI: 10.1039/b000000x/

1. P. L. Walker Jr, *Carbon*, 1972, 10, ii-382.
2. M. Pagliaro and M. Rossi, *The Royal Society of Chemistry*, 2008, Chapter 1, 1-17.
3. J. L. Figueiredo and M. F. R. Pereira, in *Carbon Materials for Catalysis*, John Wiley & Sons, Inc., 2008, pp. 177-217.
4. A. K. Geim and K. S. Novoselov, *Nat. Mater.*, 2007, 6, 183-191.
5. S. H. Friedman, *Nat. Chem.*, 2012, 4, 426-426.
6. S. Brunauer, P. H. Emmett and E. Teller, *J. Am. Chem. Soc.*, 1938, 60, 309-319.
7. A. S. Fialkov, *Russ. J. Electrochem.*, 2000, 36, 345-366.
8. J. M. Thomas, *Carbon*, 1970, 8, 413-421.
9. M. Lahmani, C. Bréchignac and P. Houdy, *Les nanosciences: 2. Nanomatériaux et nanochimie*, Belin, Paris, 2 edn., 2012.
10. C. G. Vayenas, *Interfacial Phenomena in Electrocatalysis*, Springer New York, 2011.
11. M. Shao, *Electrocatalysis in Fuel Cell*, Springer London, 2013.
12. A. Wieckowski, E. R. Savinova and C. G. Vayenas, *Catalysis and Electrocatalysis at Nanoparticle Surfaces*, Marcel Dekker, Inc., 2003.
13. R. Yu, L. Chen, Q. Liu, J. Lin, K.-L. Tan, S. C. Ng, H. S. O. Chan, G.-Q. Xu and T. S. A. Hor, *Chem. Mater.*, 1998, 10, 718-722.
14. J. B. Xu and T. S. Zhao, *J. Power Sources*, 2010, 195, 1071-1075.
15. J. Ma, A. Habrioux, N. Guignard and N. Alonso-Vante, *J. Phys. Chem. C*, 2012, 116, 21788-21794.
16. M. Simões, S. Baranton and C. Coutanceau, *J. Phys. Chem. C*, 2009, 113, 13369-13376.
17. C. Grolleau, C. Coutanceau, F. Pierre and J. M. Léger, *Electrochim. Acta*, 2008, 53, 7157-7165.
18. N. Krishnankutty and M. A. Vannice, *Chem. Mater.*, 1995, 7, 754-763.
19. D. Tashima, T. Kishita, S. Maeno and Y. Nagasawa, *Mater. Lett.*, 2013, 110, 105-107.
20. F. Gloaguen, F. Andolfatto, R. Durand and P. Ozil, *J. Appl. Electrochem.*, 1994, 24, 863-869.
21. M. K. Debe, *Nature*, 2012, 486, 43-51.
22. A. Salvatore Aricò, A. Stassi, I. Gatto, G. Monforte, E. Passalacqua and V. Antonucci, *J. Phys. Chem. C*, 2010, 114, 15823-15836.
23. J.-S. Lee, G. S. Park, H. I. Lee, S. T. Kim, R. Cao, M. Liu and J. Cho, *Nano Lett.*, 2011, 11, 5362-5366.
24. J. Speder, A. Zana, I. Spanos, J. J. K. Kirkensgaard, K. Mortensen and M. Arenz, *Electrochem. Commun.*, 2013, 34, 153-156.
25. I. Spanos, J. J. K. Kirkensgaard, K. Mortensen and M. Arenz, *J. Power Sources*, 2014, 245, 908-914.
26. Y. Kamitaka, S. Tsujimura, N. Setoyama, T. Kajino and K. Kano, *Phys. Chem. Chem. Phys.*, 2007, 9, 1793-1801.
27. H. A. Gasteiger, S. S. Kocha, B. Sompalli and F. T. Wagner, *Appl. Catal. B: Env., 2005, 56, 9-35.*
28. I. Katsounaros, S. Cherevko, A. R. Zeradjanin and K. J. Mayrhofer, *Angew. Chem. Int. Ed. Engl.*, 2014, 53, 102-121.
29. V. W. W. Yam, *Nat. Chem.*, 2010, 2, 790-790.
30. P. Tonda-Mikiela, T. W. Napporn, C. Morais, K. Servat, A. Chen and K. B. Kokoh, *J. Electrochem. Soc.*, 2012, 159, H828-H833.
31. Y. Holade, C. Morais, K. Servat, T. W. Napporn and K. B. Kokoh, *ACS Catal.*, 2013, 3, 2403-2411.
32. Y. Holade, C. Morais, S. Arrii-Clacens, K. Servat, T. W. Napporn and K. B. Kokoh, *Electrocatalysis*, 2013, 4, 167-178.
33. Y. Holade, C. Morais, T. W. Napporn, K. Servat and K. B. Kokoh, *ECS Trans.*, 2014, 58, 25-35.
34. K. Sing, D. Everett, R. Haul, L. Moscou, R. Pierotti, J. Rouquerol and T. Siemieniewska, *Pure Appl. Chem.*, 1982, 54, 2201.

Physical Chemistry Chemical Physics Accepted Manuscript

35. K. Sing, D. Everett, R. Haul, L. Moscou, R. Pierotti, J. Rouquerol and T. Siemieniewska, *Pure Appl. Chem.*, 1985, 57, 603-619.
36. T. Sumner, *Science*, 2014, 343, 1092-1093.
37. J. I. Langford, D. Louer and P. Scardi, *J. Appl. Cryst.*, 2000, 33, 964-974.
38. M. D. Abràmoff, P. J. Magalhães and S. J. Ram, *Biophotonics Int.*, 2004, 11, 36-42.
39. C. A. Schneider, W. S. Rasband and K. W. Eliceiri, *Nat. Meth.*, 2012, 9, 671-675.
40. J. C. Eklund, A. M. Bond, J. A. Alden and R. G. Compton, in *Advances in Physical Organic Chemistry*, ed. D. Bethell, Academic Press, 1999, vol. 32, pp. 1-120.
41. J. Wang, *Analytical Electrochemistry, 2nd Ed.*, John Wiley & Sons Inc., 2004.
42. Allen J. Bard and L. R. Faulkner, *Electrochemical Methods: Fundamentals and Applications*, John Wiley & Son, Inc., USA, 2nd edn., 2001.
43. M. S. Wilson, J. A. Valerio and S. Gottesfeld, *Electrochim. Acta*, 1995, 40, 355-363.
44. M. Inagaki, *New Carbon Materials*, 2009, 24, 193-232.
45. M. Nakamizo, H. Honda, M. Inagaki and Y. Hishiyama, *Carbon*, 1977, 15, 295-298.
46. G. Katagiri, H. Ishida and A. Ishitani, *Carbon*, 1988, 26, 565-571.
47. Y. Wang, D. C. Alsmeyer and R. L. McCreery, *Chem. Mater.*, 1990, 2, 557-563.
48. A. Cuesta, P. Dhamelincourt, J. Laureyns, A. Martínez-Alonso and J. M. D. Tascón, *Carbon*, 1994, 32, 1523-1532.
49. T. Jawhari, A. Roid and J. Casado, *Carbon*, 1995, 33, 1561-1565.
50. A. Sadezky, H. Muckenhuber, H. Grothe, R. Niessner and U. Pöschl, *Carbon*, 2005, 43, 1731-1742.
51. M. Veres, S. Tóth and M. Koós, *Diamond Relat. Mater.*, 2008, 17, 1692-1696.
52. J.-P. Dodelet, in *Electrocatalysis in Fuel Cells*, ed. M. Shao, Springer London, 2013, vol. 9, ch. 10, pp. 271-338.
53. L. C. Nistor, J. Landuyt, V. G. Ralchenko, T. V. Kononenko, E. D. Obraztsova and V. E. Strelnitsky, *Appl. Phys. A*, 1994, 58, 137-144.
54. M. A. Pimenta, G. Dresselhaus, M. S. Dresselhaus, L. G. Cancado, A. Jorio and R. Saito, *Phys. Chem. Chem. Phys.*, 2007, 9, 1276-1290.
55. J. Schwan, S. Ulrich, V. Batori, H. Ehrhardt and S. Silva, *J. Appl. Phys.*, 1996, 80, 440-447.
56. J. Kohanoff, *Comput. Mater. Sci.*, 1994, 2, 221-232.
57. L. G. Cançado, K. Takai, T. Enoki, M. Endo, Y. A. Kim, H. Mizusaki, A. Jorio, L. N. Coelho, R. Magalhães-Paniago and M. A. Pimenta, *Appl. Phys. Lett.*, 2006, 88, 163106.
58. R. Sellin, J.-M. Clacens and C. Coutanceau, *Carbon*, 2010, 48, 2244-2254.
59. R. Sellin, C. Grolleau, S. Arrii-Clacens, S. Pronier, J.-M. Clacens, C. Coutanceau and J.-M. Léger, *J. Phys. Chem. C*, 2009, 113, 21735-21744.
60. B. E. Warren, *X-Ray Diffraction*, Dover Publications, Inc., New York, 2nd Ed., 1990.
61. S. K. Chatterjee, *X-ray Diffraction: Its Theory and Applications*, Prentice-Hall of India Pvt.Ltd, New Delhi, India, 2nd edn., 2010.
62. M. F. Perutz, *Nature*, 1971, 233, 74-76.
63. C. Suryanarayana and M. G. Norton, eds., *X-Ray Diffraction, A Pratical Approach*, Plenum Publishing Corporation, New York, 1998.
64. H. J. Wasserman and J. S. Vermaak, *Surf. Sci*, 1972, 32, 168-174.
65. A. Habrioux, W. Vogel, M. Guinel, L. Guetaz, K. Servat, B. Kokoh and N. Alonso-Vante, *Phys. Chem. Chem. Phys.*, 2009, 11, 3573-3579.
66. A. Habrioux, E. Sibert, K. Servat, W. Vogel, K. B. Kokoh and N. Alonso-Vante, *J. Phys. Chem. B*, 2007, 111, 10329-10333.
67. W. Vogel, *J. Phys. Chem. C*, 2008, 112, 13475-13482.
68. D. Mott, J. Luo, A. Smith, P. N. Njoki, L. Wang and C.-J. Zhong, *Nanoscale Res. Lett.*, 2007, 2, 12-16.
69. B. Rogers, J. Adams and S. Pennathur, *Nanotechnology: The Whole Story*, CRC Press Inc., 2012.
70. K. J. Klabunde, *Nanoscale Materials in Chemistry*, John Wiley & Sons, Inc., 2001.
71. Q. S. Mei and K. Lu, *Prog. Mater. Sci.*, 2007, 52, 1175-1262.
72. S. Swaminarayan, R. Najafabadi and D. J. Srolovitz, *Surf. Sci*, 1994, 306, 367-380.
73. K. J. Carroll, PhD Thesis, Virginia Commonwealth University, 2010.
74. N. C. Popa and D. Balzar, *J. Appl. Cryst.*, 2002, 35, 338-346.
75. K. Kinoshita and J. A. S. Bett, *Carbon*, 1973, 11, 403-411.
76. A. Manzo-Robledo, A. C. Boucher, E. Pastor and N. Alonso-Vante, *Fuel Cells*, 2002, 2, 109-116.
77. D. Basu and S. Basu, *Electrochim. Acta*, 2010, 55, 5775-5779.
78. S. C. Barton, J. Gallaway and P. Atanassov, *Chem. Rev.*, 2004, 104, 4867-4886.
79. A. Heller and B. Feldman, *Chem. Rev.*, 2008, 108, 2482-2505.
80. E. Katz and K. MacVittie, *Energy Environ. Sci.*, 2013, 6, 2791-2803.
81. A. Habrioux, K. Servat, S. Tingry and K. B. Kokoh, *Electrochem. Commun.*, 2009, 11, 111-113.
82. K. B. Kokoh, P. Parpot, E. M. Belgsir, J. M. Léger, B. Beden and C. Lamy, *Electrochim. Acta*, 1993, 38, 1359-1365.
83. D. Basu and S. Basu, *Int. J. Hydrogen Energy*, 2011, 36, 14923-14929.

Physical Chemistry Chemical Physics Accepted Manuscript